

Suppressing Coherent Two-Qubit Errors via Dynamical Decoupling

Jiawei Qiu,^{1,2,†} Yuxuan Zhou,^{1,2,‡} Chang-Kang Hu,^{1,3,4} Jiahao Yuan,^{1,2} Libo Zhang,^{1,3,4} Ji Chu,¹ Wenhui Huang,^{1,2} Weiyang Liu,^{1,3,4} Kai Luo,^{1,2} Zhongchu Ni,^{1,2} Xianchuang Pan,¹ Zhixuan Yang,¹ Yimeng Zhang,¹ Yuanzhen Chen,^{1,2,3,4} Xiu-Hao Deng,^{1,3,4} Ling Hu,^{1,3,4} Jian Li,^{1,3,4} Jingjing Niu,^{1,3,4} Yuan Xu,^{1,3,4} Tongxing Yan,^{1,3,4} Youpeng Zhong,^{1,3,4} Song Liu,^{1,3,4,*} Fei Yan,^{1,3,4,†} and Dapeng Yu^{1,2,3,4}

¹Shenzhen Institute for Quantum Science and Engineering, Southern University of Science and Technology, Shenzhen 518055, China

²Department of Physics, Southern University of Science and Technology, Shenzhen 518055, China

³Guangdong Provincial Key Laboratory of Quantum Science and Engineering, Southern University of Science and Technology, Shenzhen 518055, China

⁴Shenzhen Key Laboratory of Quantum Science and Engineering, Southern University of Science and Technology, Shenzhen 518055, China

(Received 8 June 2021; revised 6 September 2021; accepted 18 October 2021; published 29 November 2021)

Scalable quantum information processing requires the ability to tune multiqubit interactions. This makes the precise manipulation of quantum states particularly difficult for multiqubit interactions because tunability unavoidably introduces sensitivity to fluctuations in the tuning parameters, leading to erroneous multiqubit gate operations. The performance of quantum algorithms may be severely compromised by coherent multiqubit errors. It is therefore imperative to understand how these fluctuations affect multiqubit interactions and, more importantly, to mitigate their influence. In this study, we demonstrate how to implement dynamical-decoupling techniques to suppress the two-qubit analogue of the dephasing on a superconducting quantum device featuring a compact tunable coupler, a trending technology that enables the fast manipulation of qubit-qubit interactions. The pure-dephasing time shows up to an approximate 14 times enhancement on average when using robust sequences. The results are in good agreement with the noise generated from room-temperature circuits. Our study further reveals the decohering processes associated with tunable couplers and establishes a framework to develop gates and sequences robust against two-qubit errors.

DOI: 10.1103/PhysRevApplied.16.054047

I. INTRODUCTION

High-fidelity quantum operations are key to scalable quantum information processing. For example, in the gate-based model, two-qubit gates currently constitute the performance bottleneck for noisy intermediate-scale quantum devices [1] as a result of nonidealities in physical devices, which make it extremely difficult to precisely manipulate qubit-qubit interactions. The idea of using a tunable coupler to enable independent control over the coupling strength has proven effective in recent experiments on superconducting qubit platforms [2–12], resulting in substantial improvements in the gate performance.

Despite successful demonstrations, the cost of using a tunable coupler, e.g., the new decohering processes it introduces, requires further investigation and reducing this cost

remains a challenge. In fact, fast modulation of the coupling unavoidably leads to strong sensitivity to the biasing parameter of the coupler, which, in the case of superconducting qubits, is often the magnetic flux threading a superconducting quantum interference device (SQUID) loop. Therefore, any flux fluctuations, e.g., from instrumental instabilities [13], electromagnetic interference, and the ubiquitous $1/f$ flux noise in solid-state devices [14–16], will lead to diffusion in the qubit-qubit interaction rates, compromising the two-qubit gate performance. Unfortunately, such coherent or unitary errors are often overlooked in conventional benchmarking tests based on random quantum circuits, but may build up much faster in circuits with repeated operations [17–19], as required by most quantum algorithms. It is therefore insufficient to consider only the digitized errors. More importantly, even though studies have been done on predicting surface code [20,21] performance with single-qubit coherent errors [22], two-qubit Pauli errors [21], and (static) crosstalk errors [23], it is still unclear how error-correction codes will be affected

*lius3@sustech.edu.cn

†yanf7@sustech.edu.cn

‡These two authors contributed equally.

by coherent two-qubit errors. These errors pose additional challenges to developing fault-tolerant quantum computers.

It is the need to suppress these coherent two-qubit errors that motivates studies of the noise model and related decohering processes, as well as the search for open-loop quantum control strategies, such as dynamical-decoupling (DD) techniques for error mitigation [24,25]. These techniques have been successfully implemented in various quantum systems [26–31]. In superconducting quantum circuits, decoherence mitigation has been demonstrated in a single-qubit system [32–38] and in a system consisting of a qubit and a spurious two-level system [39]. The “net-zero” technique [40] that takes advantage of specific system properties to cancel noise when performing a two-qubit gate is reminiscent of dynamical correction. However, general implementation of DD with two-qubit interactions has yet to be shown.

In this study, we extend dynamical-decoupling techniques to the realm of two-qubit interactions. The device features a tunable coupler that can continuously tune the excitation-swapping rate (absolute value) between two qubits from exactly zero to approximately 100 MHz. In the two-level subspace spanned by the Bell states, the tunable coupler introduces a nonlocal dephasing effect to the swapping operation (which we refer to as swap dephasing) as a result of low-frequency flux noise. By establishing the framework for full control over this subspace qubit, we implemented analogues of various DD sequences, demonstrating an elongation of the swap-dephasing time of up to approximately 14 times. An error analysis shows that the relevant flux noise originates from room-temperature electronics and ground loops.

II. A TUNABLE-COUPLER DEVICE

The device used in our experiment is made of aluminum on sapphire, with the metal-layer layout shown in Fig. 1(b). Our tunable coupler (C), sandwiched by two Xmon qubits (Q_1 and Q_2) [41], is a split transmon qubit that is capacitively shunted by a square-shaped pad to the ground. On the one hand, such a compact coupler design is spatially advantageous for scaling up, allowing for higher connectivity in a two-dimensional qubit array. On the other hand, the interpad capacitances [C_{1c} , C_{2c} , and C_{12} as shown in Fig. 1(c)] can be conveniently designed to achieve desirable values, enabling both strong nearest-neighbor qubit-coupler coupling ($g_{1c}/2\pi = 122$ MHz, $g_{2c}/2\pi = 105$ MHz) and strong next-nearest-neighbor direct qubit-qubit coupling ($g_{12}/2\pi = 12$ MHz), which are crucial for achieving high-fidelity two-qubit gates, as previously demonstrated with this same device [8]. Both the coupler (ω_c) and the qubit on the left (ω_1) are frequency tunable by the magnetic flux threading the SQUID loop (Φ_c and Φ_1 , respectively), while the qubit on the right has

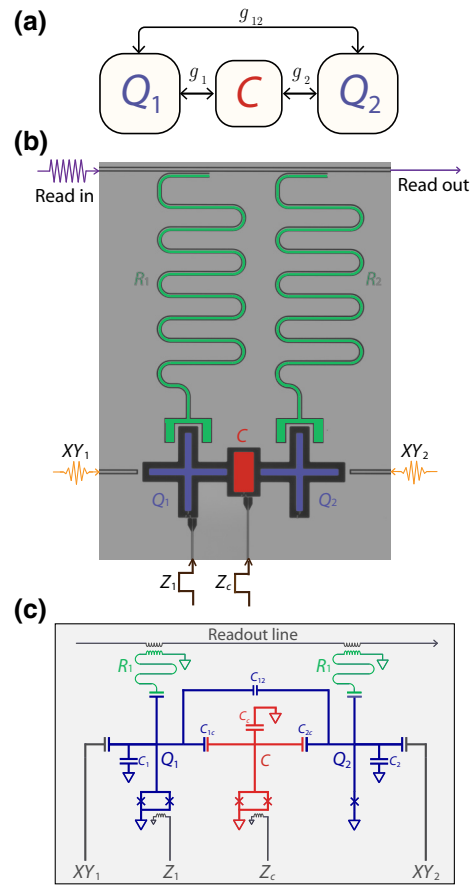


FIG. 1. The tunable-coupling architecture and a compact design. (a) Schematic of the architecture with a tunable coupler between two qubits. (b) Micrograph of the physical device implemented with superconducting quantum circuits. Two Xmon qubits (blue) and a tunable coupler (red) are capacitively connected via their shunt capacitor pads. Each qubit is connected to a quarter-wavelength transmission-line resonator (green) for dispersive readouts. The readout signal is transmitted through a common transmission line coupled to the two resonators. Both qubits have local XY drive lines for single-qubit operations. Both the left qubit and the coupler have their local flux or Z bias line for frequency tuning. (c) Circuit diagram of the device. Design values of the shunt capacitance of the qubits and the coupler are $C_1 = C_2 = 81.4$ fF and $C_c = 44.4$ fF. The qubit-coupler coupling capacitance $C_{1c} = C_{2c} = 3.3$ fF, and the qubit-qubit direct-coupling capacitance $C_{12} = 0.16$ fF.

a fixed frequency (ω_2). Relevant device parameters are listed in Table I. Both qubits have local XY drive lines (7.5 GHz bandwidth), and both Q_1 and the coupler have local Z bias lines (500 MHz bandwidth) for frequency tuning. Each qubit is connected to a quarter-wavelength resonator for dispersive readout. The chip is packaged inside an aluminum box and mounted in a dilution refrigerator (base temperature of approximately 10 mK) during measurements. See the Supplemental Material [42] for

TABLE I. Device parameters.

	Q_1	C	Q_2
Resonator frequency (GHz)	6.955	...	7.001
Qubit/coupler (max) frequency (GHz)	5.270	8.831	4.614
Qubit/coupler anharmonicity (MHz)	-222	-378	-242
Qubit/coupler idling frequency (GHz)	4.649	6.150	4.614
T_1 at max frequency (μs)	9.7	...	12.8
T_1 at idling (μs)	6.5	4.0	6.6
T_φ (Ramsey) at idling (μs)	0.7	0.3	29.3
T_φ (Echo) at idling (μs)	3.8	2.4	125.7
Qubit-coupler coupling (MHz)	—	-122—105—	—
Qubit-qubit direct coupling (MHz)	—	—12—	—

more details concerning the device design, fabrication, and the measurement setup.

Our design enables the tunable-coupling scheme previously proposed in Ref. [43], in which an exchange-type interaction acts between the $|01\rangle$ and $|10\rangle$ states. We may express their subspace Hamiltonian as

$$\mathcal{H} = \frac{1}{2}\Delta(\Phi_1)(|10\rangle\langle 10| - |01\rangle\langle 01|) + g(\Phi_c)(|10\rangle\langle 01| + |01\rangle\langle 10|), \quad (1)$$

where $\Delta(\Phi_1) = \omega_1(\Phi_1) - \omega_2$ is the qubit-qubit detuning, and $g(\Phi_c)$ is the net qubit-qubit coupling strength

$$g(\Phi_c) = g_{12} + \frac{g_{1c}g_{2c}}{2} \left(\frac{1}{\Delta_1(\Phi_c)} + \frac{1}{\Delta_2(\Phi_c)} \right), \quad (2)$$

where $\Delta_i(\Phi_c) = \omega_i - \omega_c(\Phi_c)$ ($i = 1, 2$) is the qubit-coupler detuning. It can be seen that the coupling channels are twofold: a direct coupling between qubits and an indirect coupling mediated by the coupler via virtual exchange interaction. Given negative detuning between the qubit and coupler ($\Delta_i(\Phi_c) < 0$), g can be tuned continuously from positive to negative by adjusting the coupler frequency $\omega_c(\Phi_c)$.

Equation (1) suggests that qubit excitation will cycle between $|10\rangle$ and $|01\rangle$ at the frequency $\Omega(\Phi_c) = 2g(\Phi_c)$ when $\Delta(\Phi_1) = 0$. To characterize the tunable coupling, we initialize the system to the state $|01\rangle$, pulse bias Q_1 to resonate with Q_2 , pulse bias the coupler from an idling point ($\Phi_{c,\text{idle}}$) to a certain Φ_c , and wait for a varying duration before pulsing back and measuring the final population. The data are shown in Fig. 2(a) at different flux biases referenced to the idling bias, i.e., $\Phi_{c,\text{ref}} = \Phi_c - \Phi_{c,\text{idle}}$. The fringing pattern shows the swapping dynamics between $|10\rangle$ and $|01\rangle$ with the oscillation frequency defined by $\Omega(\Phi_{c,\text{ref}})$. Notably, at $\Phi_{c,\text{ref}} = 0$ (i.e., $\Phi_c \approx 0.17\Phi_0$), the oscillations disappear, indicating that the coupling is turned off completely (we choose this bias as the idling point). The idling frequency of Q_1 is chosen to be approximately 35 MHz above ω_2 .

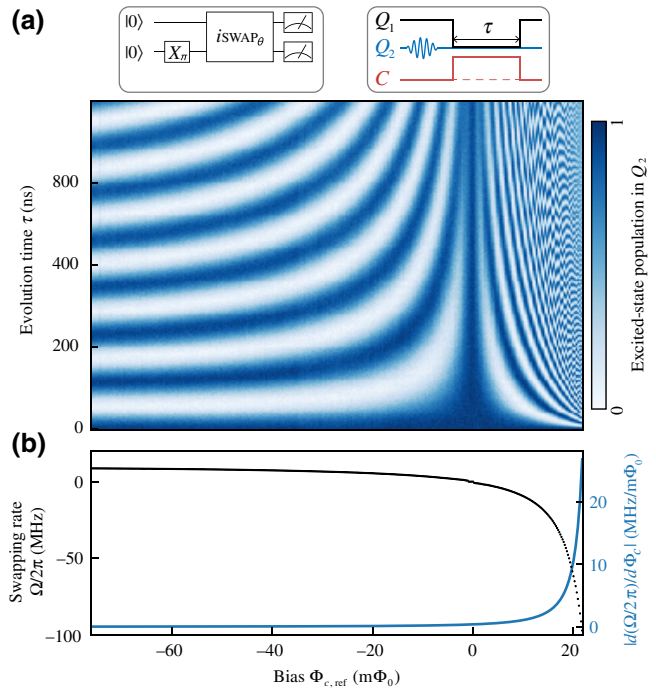


FIG. 2. Demonstration of tunable coupling. (a) Excitation swapping at different coupler bias. By preparing the system in the $|01\rangle$ state and tuning Q_1 into a resonance with Q_2 , we measure the excited-state population in Q_2 at different swapping times τ and coupler biases Φ_c . The gate sequence and corresponding waveforms are shown in the top panels. The variable swap operation is denoted as an $i\text{SWAP}_\theta$ gate, where $\theta = \Omega\tau$ is the swap angle. (b) The swapping rate $\Omega(\Phi_{c,\text{ref}})/2\pi$ dependence (black) extracted by fitting the fringes in (a), and the magnitude of its first derivative (sensitivity) to flux, $|d(\Omega/2\pi)/d\Phi_c|$.

From the oscillation frequency, we obtain the $\Omega(\Phi_{c,\text{ref}})$ dependence, which, in good agreement with theory, varies smoothly from +8.7 to -97.1 MHz over the measured range shown in Fig. 2(b). The net coupling is dominated by direct qubit-qubit coupling (positive) when the coupler frequency is far above the qubit frequency ($\Phi_{c,\text{ref}} < 0$) and by coupler-mediated virtual exchange coupling (negative) when the coupler frequency is near the qubit frequency ($\Phi_{c,\text{ref}} > 0$). At a critical value $\omega_c(\Phi_{c,\text{ref}} = 0) = 6.15$ GHz, these two effects cancel out, leading to net zero coupling. The large tunability in the coupling enables fast two-qubit operations while eliminating residual coupling during idling or single-qubit operations.

III. SWAP-DEPHASING INDUCED BY FLUX NOISE

As shown in Fig. 2(b), the sensitivity of the interaction rate to flux, $|d(\Omega/2\pi)/d\Phi_c|$, increases drastically when the coupler is biased into the negative- Ω regime. This suggests that, at the working bias for fast two-qubit operations (typically $-\Omega = 25\text{--}50$ MHz), the system also becomes

considerably more vulnerable to flux noise in the coupler SQUID loop. Fluctuations in the coupler flux lead to fluctuations in the coupler frequency and hence fluctuations in the coupling strength or the swap rate between $|01\rangle$ and $|10\rangle$. For better understanding, we rewrite Eq. (1) in the spin-1/2 Hamiltonian form

$$\mathcal{H} = \frac{1}{2}[\Omega(\Phi_c) + \delta\Omega(\Phi_c)]\sigma_Z + \frac{1}{2}[\Delta(\Phi_1) + \delta\Delta(\Phi_1)]\sigma_X, \quad (3)$$

where $\sigma_{X,Y,Z}$ are the Pauli matrices. In this representation, the basis states are Bell states $|10\rangle \pm |01\rangle$ defined by the coupling term, so we call it the *g* frame. Accordingly, the qubit-qubit coupling (Ω) is the *Z* field, while the qubit-qubit detuning (Δ) is the *X* field. Here $\delta\Omega(\Phi_c)$ and $\delta\Delta(\Phi_1)$ denote the fluctuations in the corresponding terms. In this device, flux noise is the dominant source for both *Z* and *X* noise because both Q_1 and the coupler are operated at flux-sensitive points.

Slow fluctuations in Ω cause diffusion of the angles during the swapping operation, causing the fringe amplitude to decay over time. It is easier to understand the dynamics by making an analogy with the conventional pure-dephasing phenomenon in a Ramsey or free-induction experiment [44], where fluctuations in the qubit frequency desynchronize the phase coherence. The ensemble average of these unitary errors results in transverse depolarization. We thus name the diffusion phenomenon during swap operation as swap dephasing, to reflect the nature of this error, a coherent (unitary) two-qubit iSWAP error—a non-local effect—and to indicate the similarities to single-qubit dephasing dynamics. Generally, larger-distance codes are required for correcting multiqubit errors than single-qubit errors, which adds to overheads in building a fault-tolerant quantum computer. Therefore, passive methods, such as

DD techniques, have particular importance here. Note that the swap-dephasing effect should be distinguished from another coupler-introduced decoherence channel—the participation of the coupler in the overall T_1 relaxation rate due to wave function hybridization. Actually, in our experiment, we do observe shortened T_1 relaxation times for both qubits when the coupler is biased close to qubit frequencies (Table I).

Equation (3) indicates that both *Z* field and *X* field of the *g*-frame qubit can be independently controlled (after crosstalk corrections) by local flux lines. A *Z* rotation or Ω rotation is realized by setting $\Delta = 0$ and a finite Ω for a certain amount of time. In turn, an *X* or Δ rotation is realized by setting $\Omega = 0$ and a finite Δ for a certain amount of time. Since arbitrary single-qubit operation can be synthesized with *Z* and *X* rotations, we therefore establish full control over the *g*-frame qubit. Under this framework, any single-qubit pulse sequences such as DD sequences may be directly translated and implemented in this subspace two-level system. Additional properties of the *g*-frame qubit are summarized in Table II and compared to a regular qubit.

IV. ERROR SUPPRESSION BY DYNAMICAL-DECOUPLING SEQUENCES

To understand how DD techniques work for the *g*-frame qubit, we can first look at the state evolution under the spin-echo [45] protocol with a single refocusing pulse, as shown by the Bloch-picture dynamics in Fig. 3(a). After initializing the state to $|10\rangle$ or $|01\rangle$, the system state is within the subspace (first Bloch sphere). The state of the *g*-frame qubit will precess around the longitudinal (*Z*) axis at a fluctuating rate $\Omega(\Phi_c) + \delta\Omega(\Phi_c)$. Given the usually low-frequency nature of flux noise, state vectors in different realizations precess at nonuniform rates and gradually

TABLE II. Comparison between a single-qubit system and a *g*-frame qubit encoded in the one-excitation subspace of two qubits. Interestingly, for the *g*-frame qubit, the observed relaxation rate Γ_{1g} depends not only on the averaged relaxation rates of both qubits $\bar{\Gamma}_1$, i.e., the rate at which the population leaks out of the subspace, but also on Γ_Ω , the bit-flip rate between the basis states due to the noise transverse to the eigenaxis (i.e., $\delta\Delta$ noise) at the eigenfrequency (Ω).

	Laboratory-frame qubit	<i>g</i> -frame qubit ($\Delta = 0$)
Hamiltonian	$\mathcal{H} = \frac{1}{2}\omega_q\sigma_Z$	$\mathcal{H} = \frac{1}{2}\Omega\sigma_Z$
Basis states	$ 0\rangle, 1\rangle$	$(1/\sqrt{2})(10\rangle - 01\rangle), (1/\sqrt{2})(10\rangle + 01\rangle)$
Qubit operation		
<i>Z</i> -rotation Z_θ	$\omega_q(t)\sigma_Z$	$\Omega(t)\sigma_Z$
<i>X</i> -rotation X_θ	$A(t)\cos(\omega_q t)\sigma_X$	$\Delta(t)\sigma_X$
<i>Y</i> -rotation Y_θ	$A(t)\cos(\omega_q t + \pi/2)\sigma_X$	$X_{-\pi/2}Z_\theta X_\pi/2$, in particular $Y_\pi = Z_\pi X_\pi$
Relaxation		
Decay law	$\exp[-\Gamma_1\tau]$	$\exp[-\Gamma_{1g}\tau]$
Noise source	$\Gamma_1 = \frac{1}{2}S_{\perp Z}(\omega_q)$	$\Gamma_{1g} = \bar{\Gamma}_1 + \Gamma_\Omega$, where $\bar{\Gamma}_1 = \frac{1}{2}(\Gamma_{1,Q_1} + \Gamma_{1,Q_2})$, $\Gamma_\Omega = \frac{1}{2}S_\Delta(\Omega)$
Dephasing (Gaussian)		
Decay law	$\exp[-\frac{1}{2}\Gamma_1\tau - (\Gamma_\varphi\tau)^2]$	$\exp[-(\bar{\Gamma}_1 + \frac{1}{2}\Gamma_\Omega)\tau - (\Gamma_{\varphi g}\tau)^2]$
Noise source	$S_Z(\omega)$	$S_\Omega(\omega)$, and $S_\Delta(\omega)$ when Ω is small

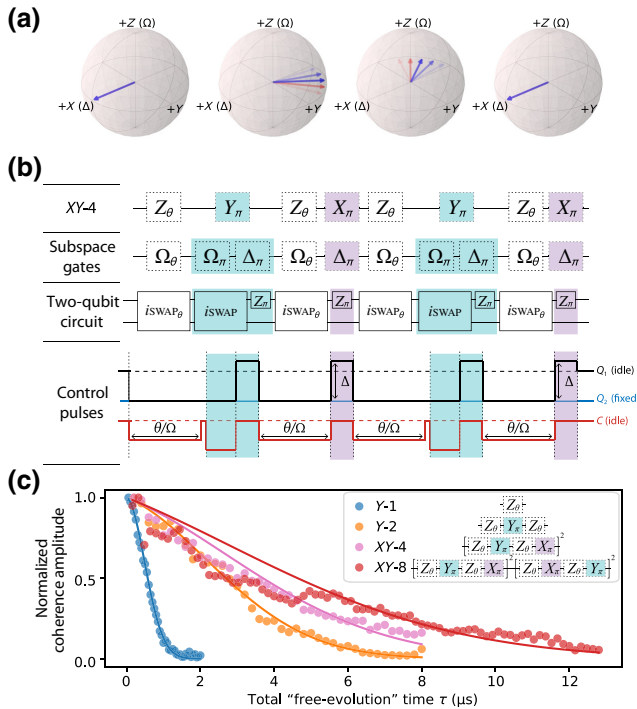


FIG. 3. Dynamical decoupling of qubit interactions. (a) Bloch picture of spin-echo evolution for the g-frame qubit with coordinates Δ , Y , and Ω , indicating the control parameters. In the second Bloch sphere, the fan out of the Bloch vectors is a consequence of the Ω -field inhomogeneities, a process analogous to single-qubit pure dephasing. After the refocusing pulse (here, an X_π pulse), the vectors converge after the same amount of evolution time. (b) Step-by-step compilation of the XY -4 sequence. The gate sequence under the single-qubit XY definition (row 1) is first translated to the Δ - Y - Ω convention (row 2); then, in the two-qubit quantum circuit (row 3), the Δ rotation is realized by a single-qubit Z rotation on Q_1 and the Ω rotation is realized by an $iSWAP$ operation; and, finally, gates are converted to control pulses (row 4). All pulses are nominally square pulses. The Ω_π gate ($\Omega = -25 \text{ MHz}$, $\tau_{\text{gate}} = 20 \text{ ns}$) and the Δ_π gate ($\Delta = 83 \text{ MHz}$, $\tau_{\text{gate}} = 6 \text{ ns}$) are precalibrated using pulse trains (see the Supplemental Material [42] for calibration details). The Ω_θ gate is an always-on free-evolution unitary, which is an $iSWAP$ -like operation with a variable swapping rate Ω and duration $\tau_\theta = \theta/\Omega$. In the experiment, we use the $YXYX$ sequence that is nominally equivalent to $XYXY$. (c) Decay of coherence amplitude measured at $\Phi_{c,\text{ref}} = 18.5 \text{ m}\Phi_0$ for various DD sequences. Note that the coherence amplitude data are full polarizations in the X - Y plane measured by a tomographylike protocol, and solid lines are decay fits of the form $f(t) = Ae^{-\tilde{\Gamma}_1 t - (\Gamma_\varphi t)^2} + B$ after correcting the beating pattern caused by the $\delta\Delta$ noise (see the Supplemental Material [42] for a discussion and correction of the noise). The inset shows the gate sequences under the XY definition, which can be compiled according to the same rule as in (b).

dephase (second Bloch sphere). At a certain time point, an X pulse, or a 180° Δ rotation flips these vectors (third Bloch sphere), which then continue to precess at the same

rate as before, such that they converge again after the same amount of evolution time as before the X pulse (fourth Bloch sphere). It can be seen that noise with correlation times longer than the free-precession period can be effectively suppressed.

In the experiment, we perform the spin-echo protocol and its generalization, periodic DD sequences [46,47], in which the free evolution is split into N equal sections by an array of refocusing pulses, e.g., $N = 1$ for Ramsey and $N = 2$ for spin echo. We also perform various types of pulse trains, including all- X , all- Y , and alternating XY pulses [48]. Figure 3(b) illustrates the compilation steps of the XY -4 sequence (XY denotes the pulse type and 4 denotes the number of split periods). In general, an X rotation is translated to a Δ rotation, while a Z rotation is translated to an Ω rotation. The Y_π gate is implemented with a composite pulse, i.e., a Z_π gate followed by an X_π gate.

Figure 3(c) shows a few selected decay traces, measured at $\Phi_{c,\text{eff}} = 18.5 \text{ m}\Phi_0$, which is in the $\delta\Omega$ -dominant regime. The results show progressive coherence improvement with more advanced sequences. Note that the displayed echo trace is taken with a Y_π pulse. Because the condition of a good refocusing pulse is a π rotation around an axis transverse to the noise axis [49], the sequence with X_π pulses is sensitive to $\delta\Delta$ fluctuations, while the sequence with a Y_π pulse is robust against both $\delta\Omega$ and $\delta\Delta$ fluctuations and is therefore a preferred choice. To further decouple the system from the noise in all directions, we use a mixture of X and Y gates such as the XY -4 and XY -8 sequences [50,51]. We find that the decay traces show stronger beating patterns with increasing N , as a consequence of the $\delta\Delta$ fluctuations that add complication to the dynamics by tilting the rotation axis (see the Supplemental Material [42] for a discussion and correction of the noise).

To disentangle the influence from the $\delta\Delta$ noise, we perform the same set of DD sequences at different flux biases. According to the filter-function formalism, the (Gaussian) pure-dephasing rate can be expressed as

$$\Gamma_\varphi = \left| \frac{d\Omega}{d\Phi_c} \right| \sqrt{\frac{1}{2\pi} \int_0^\infty d\omega S_{\Phi_c}(\omega) F(\omega, \tau^*)} = \left| \frac{d\Omega}{d\Phi_c} \right| \mathcal{A}(N), \quad (4)$$

where $S_{\Phi_c}(\omega)$ is the noise spectral density and $F(\omega, \tau^*)$ is a filter function unique to the applied DD sequence with a characteristic total duration τ^* . This integral is not sensitive to the choice of τ^* in the current case (see the Supplemental Material [42] for effects of selecting different values for τ^*). Therefore, given certain $S_{\Phi_c}(\omega)$ and τ^* , the square-root term can be treated as a function of N , $\mathcal{A}(N)$, which depends only on the type of the sequence used. From Eq. (4), the measured pure-dephasing rate Γ_φ is expected to be proportional to the noise sensitivity

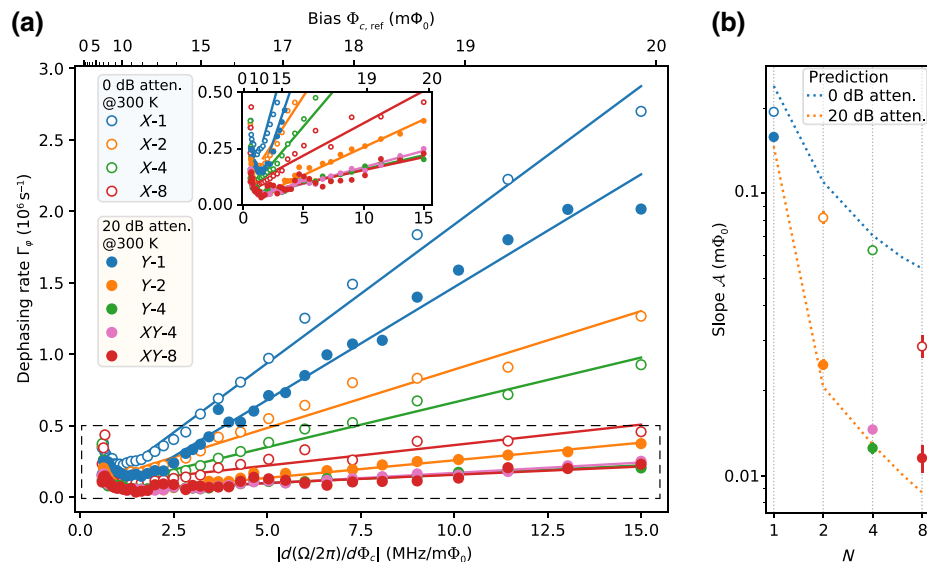


FIG. 4. Noise characterization. (a) Extracted pure-dephasing rate Γ_φ versus the flux sensitivity $d(\omega/2\pi)/d\Phi_c$ (bottom axis) or the corresponding flux biases (top axis) obtained from Fig. 2(b) for various DD sequences. Two different setups of room-temperature attenuation are used in these sequences. Note that X -1 and Y -1 are the same sequence (Ramsey). Solid lines are linear fits in the Φ_c -sensitivity regime, $d(\Omega/2\pi)/d\Phi_c \geq 1.5 \text{ MHz/m}\Phi_0$. The inset shows a magnification of the dashed area. The extracted linear slope is plotted in panel (b) for each sequence type (denoted by the number of free-induction periods N). The dashed line indicates the values estimated from the combination of directly measured signal generator noise and inferred ground-loop noise using the filter-function formalism.

$d\Omega/d\Phi_c$ in the $\delta\Phi_c$ -dominant regime. In the experiment, we measure Γ_φ at different biases to improve reliability of our model and analysis. We find good linearity for various DD sequences, which is consistent with the data shown in Fig. 4(a). The good linearity indicates that the same flux noise is responsible for observed swap-dephasing effects at different biases. The extracted slopes from linear fits are plotted in Fig. 4(b) for various DD sequences and are compared with the numerically calculated $A(N)$. A few findings regarding the performance of the DD sequences and the noise model of our system are discussed below.

To investigate the $\delta\Phi_c$ noise sources, we try two different attenuation setups, 0 and 20 dB, at room temperature over the Z control lines. As seen in Fig. 4(b), the swap-dephasing rates with the additional 20-dB attenuation are drastically smaller for $N \geq 2$. By using the filter-function formalism, we find that the abnormally strong noise in the no-attenuation case can be well explained by noise measured directly from the pulse generator. This noise is effectively suppressed by simply adding attenuation while exploiting the output range of the generator.

In the case of added 20-dB attenuation, the XY -8 sequence has generally improved the pure-dephasing time by approximately 14 times, compared to the Y -1 sequence, which demonstrates the effectiveness of using DD sequences to suppress noise in two-qubit interaction. In addition, we note that the extra attenuation shows little improvement in the $N = 1$ (Ramsey) case. We suspect the reason is extra low-frequency noise from ground loops

that cannot be attenuated (see the Supplemental Material [42] for a test of noise sources). Using a model combining both instrumentation and ground-loop noise, we find good agreement with the DD results shown in Fig. 4(b).

So far, analyses have focused on the $\delta\Phi_c$ -sensitive regime. In this regime, the strong quantization field, Ω , effectively suppresses swap dephasing from $\delta\Delta$ or $\delta\Phi_1$ noise to the second order. In the low- Ω regime, $\delta\Delta$ becomes the dominant noise source and its influence is augmented by small Ω . This explains the tilt-up of the dephasing rates towards diminishing Ω (smaller $\Phi_{c,\text{eff}}$).

V. CONCLUSION

We demonstrate a compact tunable-coupler design with a large dynamic range in a superconducting quantum circuit. Taking advantage of the full controllability over the one-excitation subspace of a two-qubit system, we implement g -frame analogues of DD sequences and demonstrate effective suppression of swap-dephasing, a type of coherent two-qubit error. The results suggest the importance of including such errors in the error model when developing fault-tolerant quantum computers. Our demonstration introduces the open-loop quantum control technique to the realm of two-qubit interactions, an important first step towards nonlocal error mitigation. Our work also establishes the framework for controlling the g -frame qubit, which can be the foundation for developing dynamically

corrected two-qubit gates [52] to further enhance system performance at large scales.

ACKNOWLEDGMENTS

We thank Simon Gustavsson, Xiaotong Ni, and Youngkyu Sung for insightful discussions, and Martha Evonuk for assistance with the editing. This work is supported by the Key-Area Research and Development Program of Guang-Dong Province (Grant No. 2018B030326001), the National Natural Science Foundation of China (U1801661), the Guangdong Innovative and Entrepreneurial Research Team Program (2016ZT06D348), the Guangdong Provincial Key Laboratory (Grant No. 2019B121203002), the Natural Science Foundation of Guangdong Province (2017B030308003), the Science, Technology and Innovation Commission of Shenzhen Municipality (JCYJ20170412152620376, KYTDPT20181011104202253), and the NSF of Beijing (Grant No. Z190012). Y.C. acknowledges support from National Natural Science Foundation of China (12074166).

Realization of High-Fidelity CZ and ZZ-Free iSWAP Gates with a Tunable Coupler, *Phys. Rev. X* **11**, 021058 (2021).

- [10] J. Stehlik, D. M. Zajac, D. L. Underwood, T. Phung, J. Blair, S. Carnevale, D. Klaus, G. A. Keefe, A. Carniol, M. Kumph, M. Steffen, and O. E. Dial, Tunable coupling architecture for fixed-frequency transmons, [ArXiv:2101.07746](https://arxiv.org/abs/2101.07746) (2021).
- [11] H. Xu, W. Liu, Z. Li, J. Han, J. Zhang, K. Linghu, Y. Li, M. Chen, Z. Yang, J. Wang, T. Ma, G. Xue, Y. Jin, and H. Yu, Realisation of adiabatic and diabatic cz gates in superconducting qubits coupled with a tunable coupler, *Chinese Physics B* (2021).
- [12] E. A. Sete, A. Q. Chen, R. Manenti, S. Kulshreshtha, and S. Poletto, Floating Tunable Coupler for Scalable Quantum Computing Architectures, *Phys. Rev. Appl.* **15**, 064063 (2021).
- [13] E. S. Fried, P. Sivarajah, N. Didier, E. A. Sete, M. P. da Silva, B. R. Johnson, and C. A. Ryan, Assessing the influence of broadband instrumentation noise on parametrically modulated superconducting qubits, [ArXiv:1908.11370](https://arxiv.org/abs/1908.11370) (2019).
- [14] F. C. Wellstood, C. Urbina, and J. Clarke, Low-frequency noise in dc superconducting quantum interference devices below 1 k, *Appl. Phys. Lett.* **50**, 772 (1987).
- [15] F. Yoshihara, K. Harrabi, A. O. Niskanen, Y. Nakamura, and J. S. Tsai, Decoherence of Flux Qubits due to \$1/f\$ Flux Noise, *Phys. Rev. Lett.* **97**, 167001 (2006).
- [16] R. C. Bialczak, R. McDermott, M. Ansmann, M. Hofheinz, N. Katz, E. Lucero, M. Neeley, A. D. O'Connell, H. Wang, A. N. Cleland, and J. M. Martinis, \$1/f\$ Flux Noise in Josephson Phase Qubits, *Phys. Rev. Lett.* **99**, 187006 (2007).
- [17] M. Kjaergaard, *et al.*, Programming a quantum computer with quantum instructions, [ArXiv:2001.08838](https://arxiv.org/abs/2001.08838) (2020).
- [18] Google AI Quantum and Collaborators, F. Arute, *et al.*, Hartree-fock on a superconducting qubit quantum computer, *Science* **369**, 1084 (2020).
- [19] A. H. Karamlou, W. A. Simon, A. Kataharwa, T. L. Scholten, B. Peropadre, and Y. Cao, Analyzing the performance of variational quantum factoring on a superconducting quantum processor, *Npj Quantum Inf.* **7**, 1 (2021).
- [20] S. B. Bravyi and A. Y. Kitaev, Quantum codes on a lattice with boundary, [ArXiv:quant-ph/9811052](https://arxiv.org/abs/quant-ph/9811052) (1998).
- [21] A. G. Fowler, M. Mariantoni, J. M. Martinis, and A. N. Cleland, Surface codes: Towards practical large-scale quantum computation, *Phys. Rev. A* **86**, 032324 (2012).
- [22] S. Bravyi, M. Englbrecht, R. König, and N. PEARL, Correcting coherent errors with surface codes, *npj Quantum Inf.* **4**, 1 (2018).
- [23] C. Huang, X. Ni, F. Zhang, M. Newman, D. Ding, X. Gao, T. Wang, H.-H. Zhao, F. Wu, G. Zhang, C. Deng, H.-S. Ku, J. Chen, and Y. Shi, Alibaba cloud quantum development platform: Surface code simulations with crosstalk, [ArXiv:2002.08918](https://arxiv.org/abs/2002.08918) (2020).
- [24] L. Viola and S. Lloyd, Dynamical suppression of decoherence in two-state quantum systems, *Phys. Rev. A* **58**, 2733 (1998).
- [25] D. Suter and G. A. Álvarez, Colloquium: Protecting quantum information against environmental noise, *Rev. Mod. Phys.* **88**, 041001 (2016).

- [26] J. Du, X. Rong, N. Zhao, Y. Wang, J. Yang, and R. B. Liu, Preserving electron spin coherence in solids by optimal dynamical decoupling, *Nature* **461**, 1265 (2009).
- [27] C. A. Ryan, J. S. Hodges, and D. G. Cory, Robust Decoupling Techniques to Extend Quantum Coherence in Diamond, *Phys. Rev. Lett.* **105**, 200402 (2010).
- [28] M. J. Biercuk, H. Uys, A. P. VanDevender, N. Shiga, W. M. Itano, and J. J. Bollinger, Optimized dynamical decoupling in a model quantum memory, *Nature* **458**, 996 (2009).
- [29] H. Bluhm, S. Foletti, I. Neder, M. Rudner, D. Mahalu, V. Umansky, and A. Yacoby, Dephasing time of gaas electron-spin qubits coupled to a nuclear bath exceeding 200 μ s, *Nat. Phys.* **7**, 109 (2011).
- [30] C. Piltz, B. Scharfenberger, A. Khromova, A. F. Varón, and C. Wunderlich, Protecting Conditional Quantum Gates by Robust Dynamical Decoupling, *Phys. Rev. Lett.* **110**, 200501 (2013).
- [31] J. Zhang and D. Suter, Experimental Protection of Two-Qubit Quantum Gates against Environmental Noise by Dynamical Decoupling, *Phys. Rev. Lett.* **115**, 110502 (2015).
- [32] J. Bylander, S. Gustavsson, F. Yan, F. Yoshihara, K. Harrabi, G. Fitch, D. G. Cory, Y. Nakamura, J.-S. Tsai, and W. D. Oliver, Noise spectroscopy through dynamical decoupling with a superconducting flux qubit, *Nat. Phys.* **7**, 565 (2011).
- [33] Q. Guo, S.-B. Zheng, J. Wang, C. Song, P. Zhang, K. Li, W. Liu, H. Deng, K. Huang, D. Zheng, X. Zhu, H. Wang, C.-Y. Lu, and J.-W. Pan, Dephasing-Insensitive Quantum Information Storage and Processing with Superconducting Qubits, *Phys. Rev. Lett.* **121**, 130501 (2018).
- [34] B. Pokharel, N. Anand, B. Fortman, and D. A. Lidar, Demonstration of Fidelity Improvement Using Dynamical Decoupling with Superconducting Qubits, *Phys. Rev. Lett.* **121**, 220502 (2018).
- [35] Y. Sung, F. Beaudoin, L. M. Norris, F. Yan, D. K. Kim, J. Y. Qiu, U. von Lüpke, J. L. Yoder, T. P. Orlando, and S. Gustavsson, Non-gaussian noise spectroscopy with a superconducting qubit sensor, *Nat. Commun.* **10**, 1 (2019).
- [36] A. M. Souza, Process tomography of robust dynamical decoupling in superconducting qubits, *Quantum Inf. Process* **20**, 237 (2021).
- [37] P. Jurcevic, *et al.*, Demonstration of quantum volume 64 on a superconducting quantum computing system, *Quantum Science and Technology*, (2021).
- [38] Z. Chen, *et al.*, Exponential suppression of bit or phase flip errors with repetitive error correction, *ArXiv:2102.06132* (2021).
- [39] S. Gustavsson, F. Yan, J. Bylander, F. Yoshihara, Y. Nakamura, T. P. Orlando, and W. D. Oliver, Dynamical Decoupling and Dephasing in Interacting Two-Level Systems, *Phys. Rev. Lett.* **109**, 010502 (2012).
- [40] M. Rol, F. Battistel, F. Malinowski, C. Bultink, B. Tarasinski, R. Vollmer, N. Haider, N. Muthusubramanian, A. Bruno, B. Terhal, and L. DiCarlo, Fast, High-Fidelity Conditional-Phase Gate Exploiting Leakage Interference in Weakly Anharmonic Superconducting Qubits, *Phys. Rev. Lett.* **123**, 120502 (2019).
- [41] R. Barends, J. Kelly, A. Megrant, D. Sank, E. Jeffrey, Y. Chen, Y. Yin, B. Chiaro, J. Mutus, C. Neill, P. O’Malley, P. Roushan, J. Wenner, T. C. White, A. N. Cleland, and J. M. Martinis, Coherent Josephson Qubit Suitable for Scalable Quantum Integrated Circuits, *Phys. Rev. Lett.* **111**, 080502 (2013).
- [42] See Supplemental Material at <http://link.aps.org/supplemental/10.1103/PhysRevApplied.16.054047> for details about the experimental setup, gate calibration, and decoherence analysis which includes reference 53–57.
- [43] F. Yan, P. Krantz, Y. Sung, M. Kjaergaard, D. Campbell, J. I. J. Wang, T. P. Orlando, S. Gustavsson, and W. D. Oliver, A Tunable Coupling Scheme for Implementing High-Fidelity Two-Qubit Gates, *Phys. Rev. Appl.* **10**, 054062 (2018).
- [44] N. F. Ramsey, A molecular beam resonance method with separated oscillating fields, *Phys. Rev.* **78**, 695 (1950).
- [45] E. L. Hahn, Spin echoes, *Phys. Rev.* **80**, 580 (1950).
- [46] H. Y. Carr and E. M. Purcell, Effects of diffusion on free precession in nuclear magnetic resonance experiments, *Phys. Rev.* **94**, 630 (1954).
- [47] S. Meiboom and D. Gill, Modified spin-echo method for measuring nuclear relaxation times, *Rev. Sci. Instrum.* **29**, 688 (1958).
- [48] T. Gullion, D. B. Baker, and M. S. Conradi, New, compensated carr-purcell sequences, *J. Magn. Reson.* (1969) **89**, 479 (1990).
- [49] T. W. Borneman, M. D. Hürlimann, and D. G. Cory, Application of optimal control to CPMG refocusing pulse design, *J. Magn. Reson.* **207**, 220 (2010).
- [50] A. M. Tyryshkin, Z.-H. Wang, W. Zhang, E. E. Haller, J. W. Ager, V. V. Dobrovitski, and S. A. Lyon, Dynamical decoupling in the presence of realistic pulse errors, *ArXiv:1011.1903* (2010).
- [51] A. M. Souza, G. A. Álvarez, and D. Suter, Robust dynamical decoupling, *philosophical transactions of the royal society A: Mathematical, Phys. Eng. Sci.* **370**, 4748 (2012).
- [52] K. Khodjasteh and L. Viola, Dynamically Error-Corrected Gates for Universal Quantum Computation, *Phys. Rev. Lett.* **102**, 080501 (2009).
- [53] M. V. Costache, G. Bridoux, I. Neumann, and S. O. Valenzuela, Lateral metallic devices made by a multiangle shadow evaporation technique, *J. Vac. Sci. Technol. B* **30**, 04E105 (2012).
- [54] A. Potts, G. J. Parker, J. J. Baumberg, and P. A. J. de Groot, Cmos compatible fabrication methods for submicron josephson junction qubits, *IEE Proc. Sci., Meas. Technol.* **148**, 225 (2001).
- [55] A. Dunsworth, *et al.*, Characterization and reduction of capacitive loss induced by sub-micron josephson junction fabrication in superconducting qubits, *Appl. Phys. Lett.* **111**, 022601 (2017).
- [56] F. Yan, S. Gustavsson, J. Bylander, X. Jin, F. Yoshihara, D. G. Cory, Y. Nakamura, T. P. Orlando, and W. D. Oliver, Rotating-frame relaxation as a noise spectrum analyser of a superconducting qubit undergoing driven evolution, *Nat. Commun.* **4**, 1 (2013).
- [57] Ł. Cywiński, R. M. Lutchyn, C. P. Nave, and S. Das Sarma, How to enhance dephasing time in superconducting qubits, *Phys. Rev. B* **77**, 174509 (2008).